Effect of Co and Ni doping on the structure, magnetic and magnetocaloric properties of Fe-rich $(Mn,Fe)_2(P,Si)$ compounds

Kiecana, A.; Batashev, I.; Dugulan, A. I.; Kwakernaak, C.; Pieter, L.; Zhang, F.; Van Dijk, N. H.; Brück, E.

DOI
10.1016/j.jmmm.2022.169710

Publication date
2022

Document Version
Final published version

Published in
Journal of Magnetism and Magnetic Materials

Journal of Magnetism and Magnetic Materials 561 (2022) 169710

Contents lists available at ScienceDirect

Journal of Magnetism and Magnetic Materials

journal homepage: www.elsevier.com/locate/jmmm

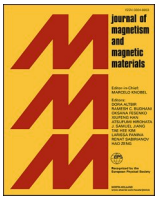

Effect of Co and Ni doping on the structure, magnetic and magnetocaloric properties of Fe-rich $(Mn,Fe)_2(P,Si)$ compounds

A. Kiecana [a,*], I. Batashev [a], A.I. Dugulan [a], C. Kwakernaak [b], L. Pieter [a], F. Zhang [a], N.H. Van Dijk [a], E. Brück [a]

[a] Fundamental Aspects of Materials and Energy Group, Department of Radiation Science and Technology, Faculty of Applied Sciences, Delft University of Technology, Mekelweg 15, 2629JB, Delft, the Netherlands

[b] Department of Materials Science and Engineering, Delft University of Technology, Mekelweg 2, 2628 CD Delft, the Netherlands

ARTICLE INFO

Keywords:
Magnetocaloric materials
Magnetic properties
Mössbauer spectroscopy
$(Mn,Fe)_2(P,Si)$

ABSTRACT

The effect of Co and Ni doping on the structure, magnetic and magnetocaloric properties of Fe-rich $(Mn,Fe)_2(P,Si)$ compounds was studied. With increasing Co and Ni content, both the Curie temperature (T_c) and the thermal hysteresis (ΔT_{hys}) decreased, whereas the hexagonal *P-62 m* crystal structure was maintained. A pronounced reduction in hysteresis was observed upon Co doping, while a significant reduction in Curie temperature was found upon Ni doping. Mössbauer spectroscopy measurements and DFT calculations indicated the substitution of Fe at the *3f* site for both Co and Ni doping. Rietveld refinement of the X-ray diffraction data showed that Co substitute atoms in the main phase and the impurity phase, while Ni exhibits an affinity to the main phase. Magnetization measurements on the Co doped samples revealed an increase in magnetization for 2 at.% of Co, followed by a decrease for higher concentrations. DFT calculations showed that the magnetic moment on the *3f* site is enhanced by Co substitution, whereas an opposite trend was observed for Ni substitution.

1. Introduction

Magnetic refrigeration based on the magnetocaloric effect (MCE) has a high potential to become a sustainable alternative for traditional compressor-based refrigeration. Systems using magnetocaloric materials (MCM) offer many advantages when compared to well-established cooling technologies. The efficiency of the compressor-based refrigerators originally developed in the 19th century saturates around 40 % of Carnot efficiency. In contrast, with magnetic cooling, it is viable to reach 60 % of Carnot efficiency, leading to significantly reduced energy consumption. In addition to this, systems that use MCMs do not involve hazardous, ozone-depleting gases, and the noise is reduced due to the elimination of compressors [1–4]. These advantages and the need for exploring environmentally-friendly technologies make magnetic cooling a very promising replacement for conventional gaseous-refrigerant-based systems.

Promising and applicable magnetocaloric materials should comply with several requirements: they should exhibit a large MCE in the proper temperature range and in low magnetic fields, since the maximum required magnetic field is directly related to cost to generate the magnetic field by permanent magnets. MCMs should also consist of non-toxic, abundant, non-critical, and readily available elements. Additionally, promising materials should display mechanical and chemical stability, a large saturation magnetization (M_s), high thermal conductivity, low specific heat and a large temperature span [5]. Among all known MCMs, the generic $(Mn,Fe)_2(P,Si)$ family that crystallizes in the hexagonal Fe_2P-type structure appears to be one of the most promising [6]. The Mn-rich compounds have been explored extensively since it was found that in this region it is feasible to obtain materials with a small hysteresis and yet exhibiting a giant magnetocaloric effect (GMCE) near room temperature [6–8]. However, as reported by Ou et al. [9,10], the Fe-rich region of the $(Mn,Fe)_2(P,Si)$ system can potentially also be favorable since compounds with a higher Fe content can show an even larger magnetic moment compared to Mn-rich materials.

The $(Mn,Fe)_2(P,Si)$ family of compounds consists of neither toxic nor expensive elements. However, controlling the thermal hysteresis originating from the first-order magnetic transition (FOMT) is a prerequisite for practical applications. The character of the transition and the

* Corresponding author at: Fundamental Aspects of Materials and Energy Group, Department of Radiation Science and Technology, Faculty of Applied Sciences, Delft University of Technology, Mekelweg 15, 2629JB, Delft, The Netherlands..

E-mail address: A.Kiecana@tudelft.nl (A. Kiecana).

https://doi.org/10.1016/j.jmmm.2022.169710
Received 15 February 2022; Received in revised form 8 June 2022; Accepted 13 July 2022
Available online 16 July 2022

magnitude of hysteresis can be tuned by utilizing appropriate doping, e.g., V, B, C, N, and changes in the heat treatment [11–16]. Various studies show that Co doping of $(Mn,Fe)_2(P,Si)$ compounds can effectively reduce the thermal hysteresis and the transition temperature [5,17,18]. Nevertheless, due to the high criticality of Co, ethical issues, and a high price, it is essential to minimize the use of Co and look for possible replacements [19]. Recent research shows that Ni can be a good alternative for Co as it leads to similar tuning effects on ΔT_{hys} and T_c [17,18,20]. However, the substitution of Co and Ni for Mn in the Fe-rich $(Mn,Fe)_2(P,Si)$ alloys has not yet been studied. Therefore, in this work, we present experimental results on Co and Ni substitution for Mn focussing on the magnetic, magnetocaloric, and structural properties of Fe-rich $(Mn,Fe)_2(P,Si)$ compounds.

2. Experimental

2.1. Sample preparation

Polycrystalline $(Mn,Fe,Co)_{1.95}(P,Si)$ and $(Mn,Fe,Ni)_{1.95}(P,Si)$ compounds were prepared by high-energy ball-milling under Ar atmosphere and subsequent solid-state reactions. We prepared two series of samples: $Mn_{0.62-x}Fe_{1.33}Co_xP_{0.66}Si_{0.34}$ and $Mn_{0.62-x}Fe_{1.33}Ni_xP_{0.66}Si_{0.34}$ ($0 \leq x \leq 0.12$). Stoichiometric proportions of powders: Mn (99.7%), Fe (99.0%), Fe_2P (99.5%), Si (99.7%), Co (99.8%), Ni (99.9%), were weighed, mixed, and ball milled by a Fritsch Pulverisette planetary ball-mill for 10 h with a constant speed of 350 rpm. Approximately 2 g of ball-milled powder was pressed into pellets and subsequently sealed in quartz tubes in 200 mbar protective Ar atmosphere. As-prepared samples were annealed at 1373 K for 20 h and finally quenched into water. In order to eliminate the so-called "virgin effect" originating from the metastability of the quenched phase, all samples were pre-cooled in liquid nitrogen before being manually powdered [21].

2.2. Instrumental methods

Transmission ^{57}Fe Mössbauer spectra were collected at 350 and 130 K with a conventional constant-acceleration spectrometer with a sinusoidal velocity spectrometer, using a ^{57}Co(Rh) source. The Mössbauer spectra were fitted with a binomial distribution model as described earlier for $FeMnP_{1-x}As_x$ using the Mosswinn 4.0 program [22].

The X-ray diffraction patterns were collected using a PANalytical X-pert Pro diffractometer with Cu-K_α radiation (1.54056 Å). Structural parameters were obtained by Rietveld refinement implemented in the Fullprof software [23].

Electron Probe Micro Analysis (EPMA) measurements were conducted with a JEOL JXA 8900R microprobe using an electron beam with energy of 10 keV and beam current of 200nA employing Wavelength Dispersive Spectrometry (WDS). The obtained intensity ratios were processed with a matrix correction program CITZAF [24].

Magnetic measurements were conducted using superconducting quantum interference devices (SQUID) MPMS-XL and MPMS-5S magnetometers, in the temperature range of 5–370 K with a constant sweep rate of 2 K/min in applied magnetic fields up to 5 T.

The differential scanning calorimetry (DSC) measurements were carried out using a TA-Q2000 DSC with a constant sweep rate of 10 K/min.

2.3. Computational methods

In this work, the preferred site occupancy of the doping atoms and the change in the local magnetic moments has been computed for $Mn_{0.62-x}Fe_{1.33}Co_xP_{0.66}Si_{0.34}$ and $Mn_{0.62-x}Fe_{1.33}Ni_xP_{0.66}Si_{0.34}$, within the framework of density functional theory (DFT). The Vienna Ab Initio simulation package (VASP) [25,26], in the projected augmented wave (PAW) method [27,28], was employed to perform the DFT calculations using the generalized gradient approximation of Perdew-Burke-Ernzerhof (PBE) for the exchange correlation functional [29]. The following orbitals were treated as valence electrons: *3p*, *3d* and *4s* for Mn; *3d* and *4s* for Fe, Ni and Co; *3s* and *3p* for P and Si.

The ***k***-space integrations were performed with the Methfessel-Paxton method [30] of second order with a smearing width of 0.05 eV. The lattice parameters and atomic positions were relaxed for a force convergence of 0.1 meV/Å, while the energies were converged to 1 μeV. The kinetic energy cut-off was set at 400 eV for all calculations. Calculations to determine the site preference for the Ni and Co atoms were performed using a $2 \times 2 \times 1$ supercell. The structural degrees of freedom were fully relaxed on a gamma centred ***k***-grid of $5 \times 5 \times 11$. For the undoped system, the obtained lattice parameters were $a = 6.12$ Å and $c = 3.26$ Å. To study the effect of the dopants on magnetic properties in this system, a $2 \times 2 \times 4$ supercell was utilized with a $5 \times 5 \times 5$ ***k***-grid. For the band structure and the density of state calculations (DOS) a smaller $2 \times 1 \times 1$ supercell with the composition $Mn_{0.66}Fe_{1.25}P_{0.66}Si_{0.33}T_{0.08}$ (T = Ni, Co) and ***k***-grid of $5 \times 7 \times 11$ was used. For the DOS calculations the ***k***-space integrations were performed with the tetrahedron method.

3. Results and discussion

In the $(Mn,Fe)_2(P,Si)$ family of compounds, Mn atoms show a preference to the pyramidal *3g* site, which is marked by a larger magnetic moment, whereas Fe atoms preferentially occupy *3f* sites, associated with a smaller magnetic moment [7,31]. In the Fe-rich region, the *3f* site is fully occupied by Fe, and the *3g* site is partially occupied by Mn and partially by Fe [32]. A schematic representation of the crystal structure is shown in Fig. 1. As proven by density functional theory (DFT) calculations, the magnetic moment of Fe at the *3g* site is lower than for the preferential Mn atoms at the same site [32,33].

3.1. Hyperfine field interactions

Mössbauer spectroscopy was carried out for a reference sample and three other samples containing Co (0, 4, 6, 12 at.%). The Mössbauer spectra recorded at 350 and 130 K are shown in Fig. 2. In the high-temperature paramagnetic (PM) phase, a single broad absorption line can be seen. In the low-temperature ferromagnetic (FM) phase, a more complex absorption profile is observed that includes six broad spectral lines, indicating a distribution in hyperfine field. Due to the fact that atoms of P and Si are randomly distributed over the *2c* and *1b* sites, slightly different sextets are observed in the FM state, reflecting the five inequivalent neighbours of the Fe atoms [22]. All fitted Mössbauer parameters, including the hyperfine fields and spectral contributions, are given in Table 1.

The aim of performed Mössbauer spectroscopy was to elucidate the influence of the Co substitution on the magnetic properties. In the Fe-rich region, the tetrahedral *3f* site is fully occupied by Fe atoms. The hyperfine field is found to decrease at this site, as indicated in Table 1. This indicates the substitution by Co, which has a significantly smaller magnetic moment at the *3f* site than the Fe atoms [33]. Alternatively, Fe might be substituted by Co at both sites, as it would lead to similar changes of the hyperfine field. However, this possibility is less likely to occur since the substitution of Fe by Co at the *3f* site was also confirmed by DFT calculations. The observed hyperfine field decrease at the pyramidal *3g* site originates from the diminishing amount of Mn in Co-doped samples and increasing amount of Fe at the *3g* Wyckoff position, which is associated with a significantly lower magnetic moment. Additionally, for the sample with the highest Co concentration (12 at.%), we observe the formation of an additional structure, most likely Fe-Co, which suggests that the limit for maximum Co substitution was reached.

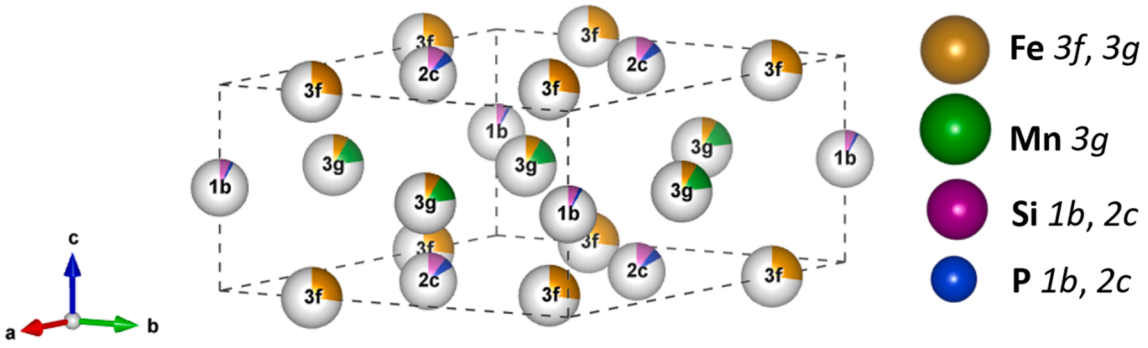

Fig. 1. Schematic representation of the crystal structure with the atom occupancy (from DFT) of the parent compound $Mn_{0.62}Fe_{1.33}P_{0.66}Si_{0.34}$.

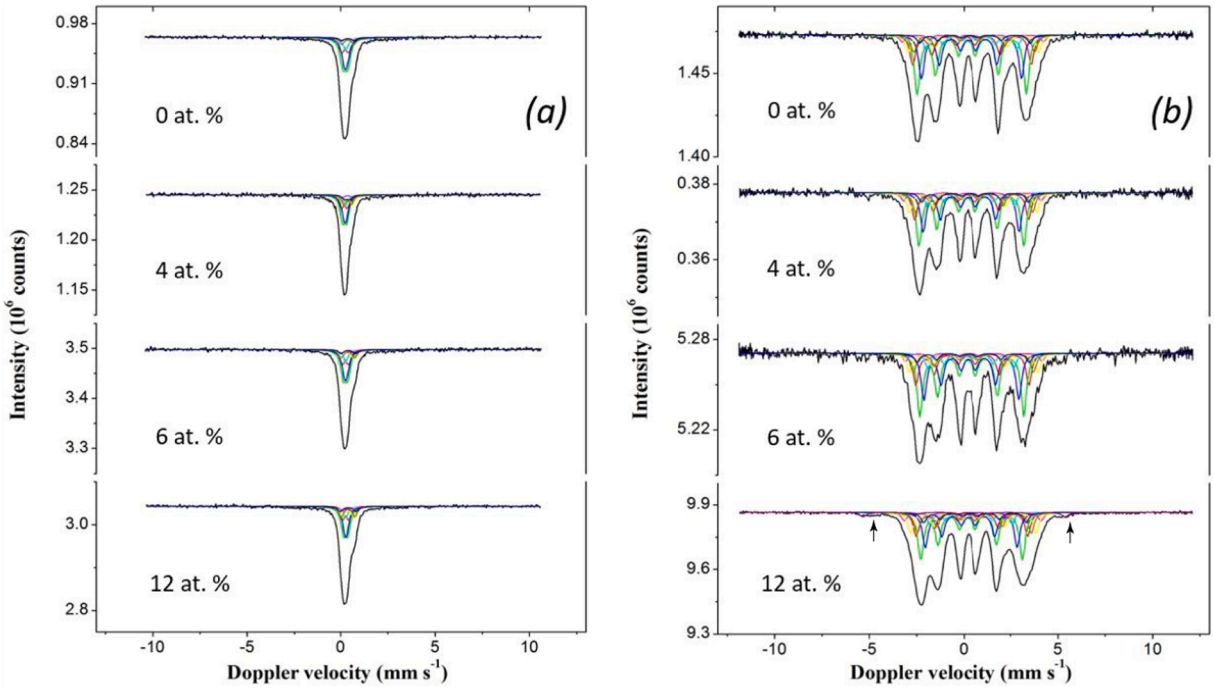

Fig. 2. Mössbauer spectra obtained for $Mn_{0.62-x}Fe_{1.33}Co_xP_{0.66}Si_{0.34}$ (x = 0, 4, 6, 12 at.%) measured at (a) 350 K and (b) 130 K.

Table 1
Mössbauer fitted parameters of $Mn_{0.62-x}Fe_{1.33}Co_xP_{0.66}Si_{0.34}$ in the PM (350 K) and the FM (130 K) state.

Atomic percent of Co (%)	*T (K)*	*IS* (mm·s^{-1})*	*QS* (mm·s^{-1})*	*Hyperfinefield* (T)*	*Γ (mm·s^{-1})*	*Phase*	*Spectral contribution (%)*
0	350	0.25	0.22	–	0.35	P1 (*3f* site)	77
		0.38	0.66	-	0.35	P2 (*3g* site)	23
	130	0.31	0.23	17.5	0.35	F1 (*3f* site)	74
		0.43	0.22	21.0	0.35	F2 (*3g* site)	26
4	350	0.24	0.19	–	0.29	P1 (*3f* site)	69
		0.36	0.50	-	0.29	P2 (*3g* site)	31
	130	0.30	0.21	16.8	0.34	F1 (*3f* site)	70
		0.40	0.24	20.5	0.34	F2 (*3g* site)	30
6	350	0.26	0.20	–	0.33	P1 (*3f* site)	68
		0.36	0.68	-	0.33	P2 (*3g* site)	32
	130	0.32	0.21	16.7	0.35	F1 (*3f* site)	63
		0.40	0.24	20.7	0.35	F2 (*3g* site)	27
12	350	0.27	0.19	–	0.36	P1 (*3f* site)	66
		0.38	0.66	-	0.36	P2 (*3g* site)	34
	130	0.31	0.20	16.3	0.35	F1 (*3f* site)	64
		0.42	0.23	20.0	0.35	F2 (*3g* site)	33
		0.28	−0.51	33.3	0.35	F3	3

Experimental uncertainties: Isomer shift: I.S. ± 0.01 mm s^{-1}; Quadrupole splitting: Q.S. ± 0.01 mm s^{-1}; Line width: Γ ± 0.01 mm s^{-1}; Hyperfine field: ± 0.1 T; Spectral contribution: ± 3%; F/P: ferromagnetic/paramagnetic phases.

3.2. Structural and microstructural characterisation

The X-Ray diffraction (XRD) patterns of Co and Ni-doped samples measured at 348 K clearly indicate that all samples crystallize in the hexagonal Fe_2P-type structure (space group *P-62m*). A Rietveld refinement of the XRD data for the parent compound is shown in Fig. 3. All samples were measured in the PM state, i.e., well above their transition temperature. Although the metal-deficiency stoichiometry was applied in order to prevent the formation of the cubic $(Mn,Fe)_3Si$ impurity phase (space group *Fm-3m*) [34], Rietveld refinement of the measured XRD patterns confirmed the presence of a small fraction (<4 wt%), of a metal-rich impurity phase in each sample, and a minor amount (~1 wt%) of Fe-Co impurity phase in $Fe_{1.33}Mn_{0.50}Co_{0.12}P_{0.66}Si_{0.35}$, which is in agreement with Mössbauer results. The excessive amount of metal content was also confirmed by EPMA measurements performed for Co and Ni-doped samples (x = 0.06, 0.12). As presented in Table 2, a significantly higher metal to non-metal (M/NM) ratio is observed in the selected samples, which prompts the occurrence of the metal-rich $(Mn,Fe)_3Si$ impurity phase. The impurity phase is present in the form of micro-sized inclusions (Fig. S1 in the Supplementary Material). The results obtained from XRD and EPMA measurements indicate that further optimization of $(Mn,Fe)_2(P,Si)$ is necessary to avoid the impurity phase.

The unit cell volume of the primary phase decreased gradually with increasing Co and Ni content since both of these elements have a smaller covalent radius than the substituted atoms: the covalent radii for Co and Ni are 1.26 and 1.24 Å, while they are significantly larger for Fe and Mn with values of 1.39 and 1.32 Å for Mn and Fe, respectively. The decrease in unit-cell volume upon doping confirms the substitutional effect of these elements. It is noticeable that with increasing Co content, the unit-cell volume of the $(Mn,Fe)_3Si$ impurity phase exhibits a similar trend as the main phase. On the contrary, the unit-cell volume of the impurity phase present in the $Mn_{0.62-x}Fe_{1.33}Ni_xP_{0.66}Si_{0.34}$ series does not significantly change, indicating that Ni exhibits a strong affinity to the main phase (Fig. 4). The preference of Co to both – the main phase and the impurity phase might contribute to a slightly diminished effect on the decrease in T_c when compared to the Ni-doped samples. As proposed by Dung et al., the relation between the c/a ratio and T_c reflects changes in the atomic distances upon doping [35]. It can be seen in Fig. 5a that the c/a ratio increases with Co content and is accompanied by the decrease in T_c, remaining almost constant beyond 8 at.% of doping. In contrast to the Co-doped samples, as depicted in Fig. 5b, the Ni-doped samples show that T_c and c/a changes linearly in the opposite sense. From the XRD patterns it is found that in $Mn_{0.62-x}Fe_{1.33}Ni_xP_{0.66}Si_{0.34}$ series, with increasing Ni content, the (300) and (002) reflections shift towards each other, indicating that the lattice parameters a and c move in the opposite sense (Fig. 6).

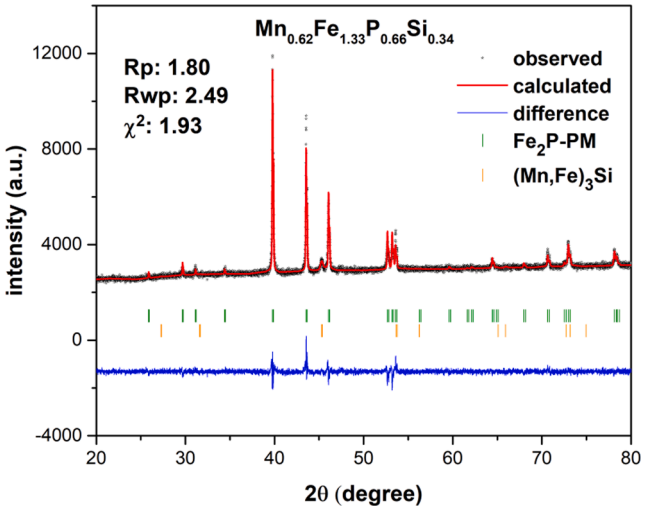

Fig. 3. Observed and calculated XRD patterns of $Mn_{0.62}Fe_{1.33}P_{0.66}Si_{0.34}$.

3.3. Magnetic properties

The temperature-dependent magnetization for the $Mn_{0.62-x}Fe_{1.33}Co_xP_{0.66}Si_{0.34}$ and $Mn_{0.62-x}Fe_{1.33}Ni_xP_{0.66}Si_{0.34}$ compounds measured in 1 T is shown in Fig. 7. It is found that T_c decreases with increasing Co and Ni content, which is in good agreement with results published by van Thang et al. [17] and Ou et al. [18]. In $Mn_{0.62-x}Fe_{1.33}Co_xP_{0.66}Si_{0.34}$, we observe that T_c and the thermal hysteresis decrease linearly up to 6 at.% Co doping and do not significantly change after exceeding the beforementioned concentration. As obtained from the DSC measurements, upon 12 at.% of Co doping, T_c decreased from 308.4 to 283.3 K and the thermal hysteresis decreased from 11.0 to 3.9 K. In $Mn_{0.62-x}Fe_{1.33}Ni_xP_{0.66}Si_{0.34}$, the thermal hysteresis also reaches a constant value for approximately 6 at.% of Ni, however the change in T_c is not retained. In the Ni-doped samples T_c changed from 308.4 to 226.6 K for 12 at.% of doping, and the thermal hysteresis decreased from 11.0 to 4.9 K. These results are consistent with the observed behaviour for the c/a ratio derived from XRD measurements. The effect of a reduced hysteresis was more pronounced in Co-doped samples, as depicted in Fig. 8. The thermal hysteresis is controlled by the energy barrier for nucleation and thus, provides an important insight into the effect of doping on the character of the magnetic transition. The decrease in the hysteresis upon doping relates to the electronic configuration of Co and Ni, as both of these atoms have an incomplete *3d* orbital and a filled *4s* orbital (7 and 8 of *3d* electrons, for Co and Ni respectively), contributing to the weakening of the energy barrier for nucleation [5,18]. As the energy barrier for nucleation is reduced, the FOMT weakens accordingly. In both series of samples, the changes in T_c and the thermal hysteresis are accompanied by the gradual decrease in the latent heat, from 6.2 kJ/kg to 0.9 kJ/kg and 0.7 kJ/kg for 12 at.% of Co and Ni doping, respectively. The changes in the latent heat and thermal hysteresis clearly indicate that dopant atoms weaken the strength of the first-order magnetic transition.

The insert of the Fig. 7a presents the field dependence of the saturation magnetization (M_s) for the $Mn_{0.62-x}Fe_{1.33}Co_xP_{0.66}Si_{0.34}$ samples. It shows that M_s increases and reaches a maximum well above the reference value for 2 at.% Co, before the decrease. As shown in Fig. 7b, for the $Mn_{0.62-x}Fe_{1.33}Ni_xP_{0.66}Si_{0.34}$ samples, the trend of increasing magnetization for a small doping is not observed. This behaviour suggests that Fe–rich $(Mn,Fe,Co)_{1.95}(P,Si)$ alloys might exhibit a similar magnetic behaviour as the Fe-Co alloys. Various studies show that the average magnetic moment of Fe-Co alloy reaches the highest value for a small Co content (20–25 at.%) before a decrease is observed [36–38]. The reason responsible for a rapid increase in M_s for a small Co doping is complex and is related to changes in the magnetic moment and electronic structure [39]. When a Co atom is respectively replacing an Fe atom with 8 e^- in the outermost shells, the structure gathers an additional *3d* e^-. The abrupt change in the saturation magnetization is explained by the increase in the mean magnetic moment caused by the enhancement of the magnetic moment of Fe, whereas the magnetic moment of Co remains almost unchanged [37,38].

3.4. DFT calculations

DFT calculations were performed in order to investigate the preferential doping site and the change in the local magnetic moments in the Fe-rich $(Mn,Fe,Co)_{1.95}(P,Si)$ and $(Mn,Fe,Ni)_{1.95}(P,Si)$ compounds. To investigate the site preference, dopant atoms were placed on either *3g* or *3f* crystallographic sites. The energy cost of forming each structure (E_f) is calculated as the difference between energies of doped (E_d) and pure (E_p) compounds, including the chemical potential contribution of the dopant atom (μ_d) and substituted atom (μ_s), as indicated in Eq. (1). The chemical potentials are obtained by first optimizing the structure for each element and then taking the value of total energy per atom.

Table 2
Aimed and found compositions, and M/NM ratios of Co and Ni-doped samples.

Sample		*Aimed Composition Main Phase*	*Found Composition Main phase*	*Ratio M/NM*
Doping type	*Content (x)*			
Co	0.06	$Fe_{1.33}Mn_{0.56}Co_{0.06}P_{0.66}Si_{0.34}$	$Fe_{1.37}Mn_{0.61}Co_{0.06}P_{0.64}Si_{0.31}$	2.04/0.95
	0.12	$Fe_{1.33}Mn_{0.50}Co_{0.12}P_{0.66}Si_{0.34}$	$Fe_{1.38}Mn_{0.55}Co_{0.12}P_{0.64}Si_{0.31}$	2.05/0.95
Ni	0.06	$Fe_{1.33}Mn_{0.56}Ni_{0.06}P_{0.66}Si_{0.34}$	$Fe_{1.38}Mn_{0.62}Ni_{0.06}P_{0.65}Si_{0.30}$	2.06/0.95
	0.12	$Fe_{1.33}Mn_{0.50}Ni_{0.12}P_{0.66}Si_{0.34}$	$Fe_{1.37}Mn_{0.54}Ni_{0.12}P_{0.65}Si_{0.33}$	2.03/0.98

The counting error: Fe and Mn – 0.15 wt%; Si, P, Co, Ni – 0.05 wt%.

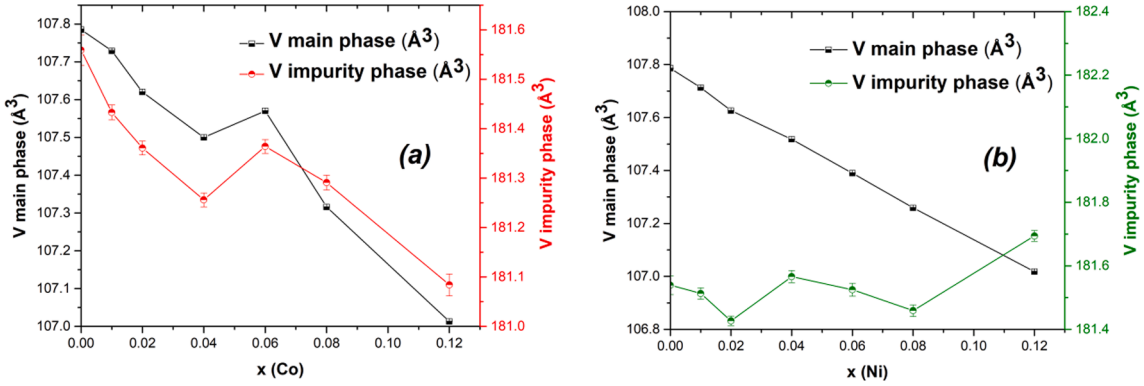

Fig. 4. Composition dependence of the volume (main phase and impurity phase) of the (a) $Mn_{0.62-x}Fe_{1.33}Co_xP_{0.66}Si_{0.34}$ and (b) $Mn_{0.62-x}Fe_{1.33}Ni_xP_{0.66}Si_{0.34}$ derived from X-ray diffraction patterns measured at 348 K (PM state).

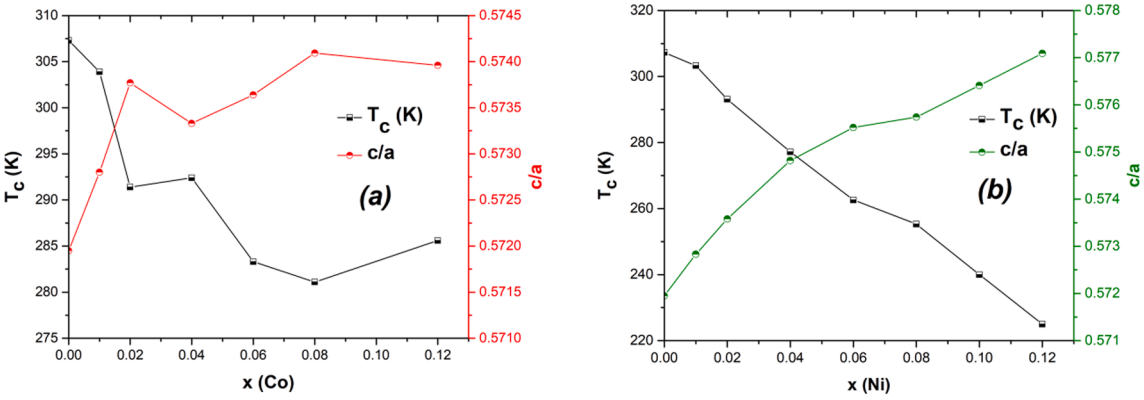

Fig. 5. Composition dependence of the T_c upon heating and c/a ratio derived from X-ray diffraction patterns measured at 348 K (PM state) of the (a) $Mn_{0.62-x}Fe_{1.33}Co_xP_{0.66}Si_{0.34}$ and (b) $Mn_{0.62-x}Fe_{1.33}Ni_xP_{0.66}Si_{0.34}$.

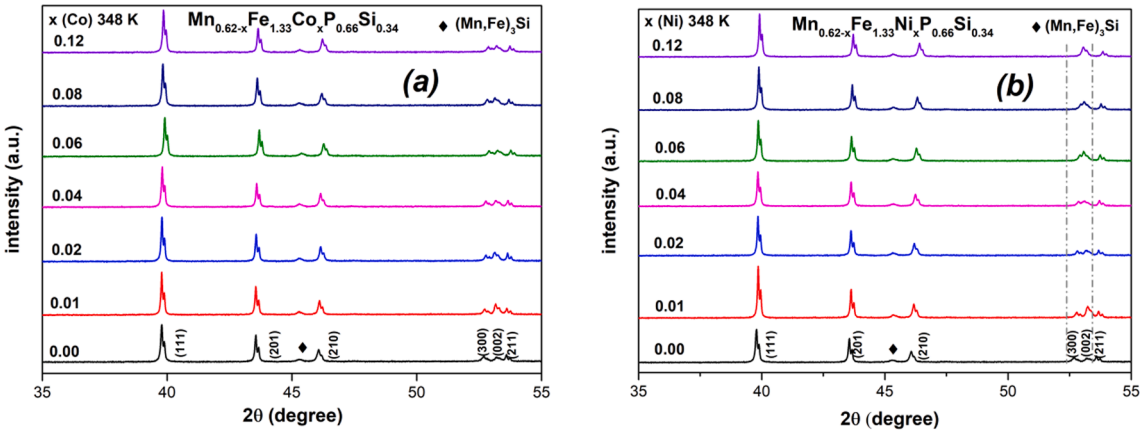

Fig. 6. X-ray diffraction patterns of (a) $Mn_{0.62-x}Fe_{1.33}Co_xP_{0.66}Si_{0.34}$ and (b) $Mn_{0.62-x}Fe_{1.33}Ni_xP_{0.66}Si_{0.34}$ recorded at 348 K (PM state). With increasing Ni content, the (300) and (002) reflections shift towards each other, indicating that the lattice parameters a and c move in opposite direction.

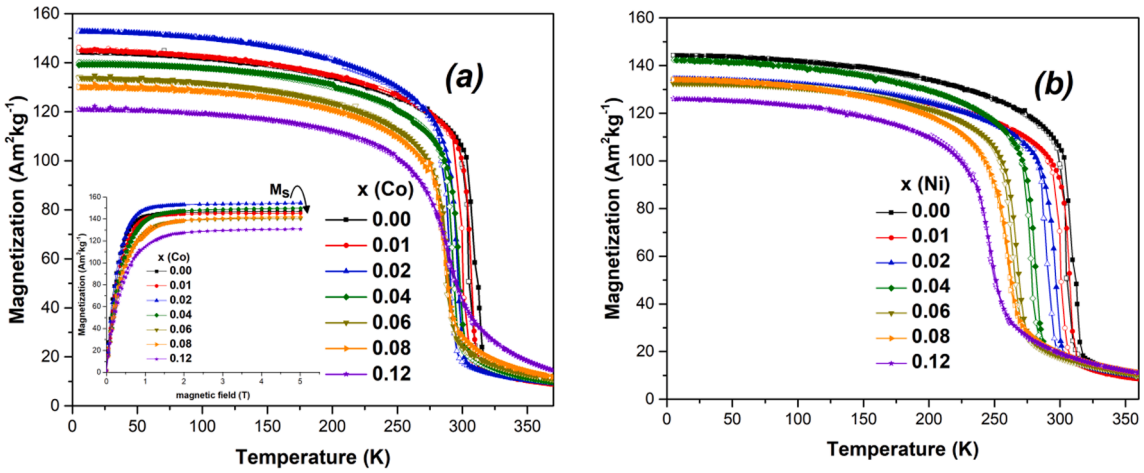

Fig. 7. Temperature dependence of the magnetization of (a) $Mn_{0.62-x}Fe_{1.33}Co_xP_{0.66}Si_{0.34}$ and (b) $Mn_{0.62-x}Fe_{1.33}Ni_xP_{0.66}Si_{0.34}$ compounds measured in a magnetic field of 1 T. The insert shows the field dependence of $Mn_{0.62-x}Fe_{1.33}Co_xP_{0.66}Si_{0.34}$ measured at 5 K.

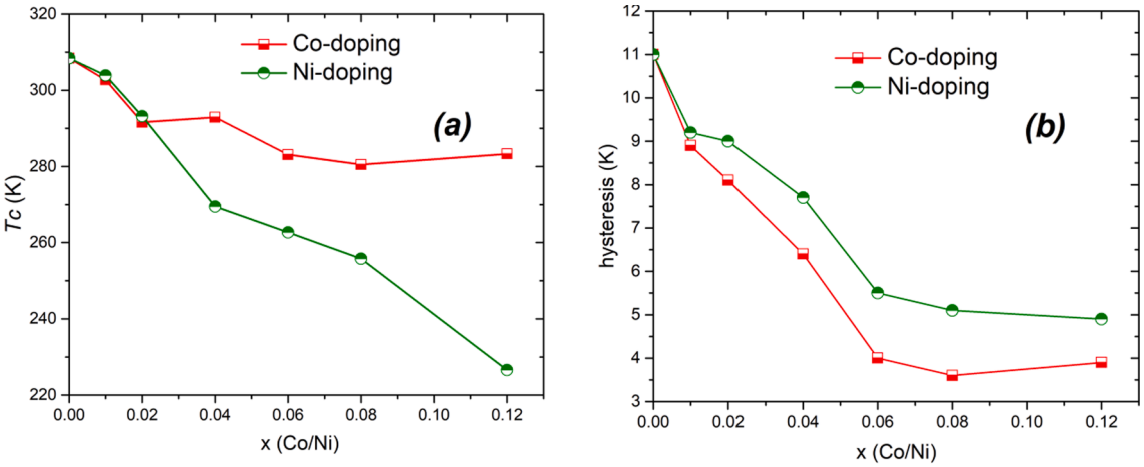

Fig. 8. (a) The composition dependence of the T_c for Co and Ni doped samples and (b) changes in the thermal hysteresis as the function of doping content obtained from DSC measurements.

$$E_f = E_{doped} + \mu_s - \left(E_{pure} + \mu_d\right) \quad (1)$$

To investigate the favorable site for the doping atoms, one Fe atom from the *3f* site was substituted and subsequently, one Mn/Fe atom from the *3 g* site by a dopant atom. From the DFT calculations, we see in Table 3 that for both – Co and Ni doping, the lowest formation energy is assigned to the *3f* site, indicating that Co and Ni substitute Fe at this site. These calculations support the findings of Mössbauer spectroscopy results discussed in section 3.1. Earlier studies have shown that correlation effects in the $(MnFe)_2(P,Si)$ family of compounds have no remarkable impact on the magnetic properties and electronic structure [40]. However, according to the previous DFT calculations [33,41], the unusual magnetocaloric properties of the $(Mn,Fe)_2(P,Si)$ across the ferromagnetic transition arise from the "mixed magnetism", which indicates the presence of an electron instability of the *3f* moments in the presence of stable *3g* moments. The magnitude of the Co and Ni magnetic moment at the *3f* site is remarkably lower in comparison to that of the substituted Fe, mainly due to the fact that the dopant atoms have more *3d* valence electrons. DFT calculations revealed that the total magnetic moment decreases with increasing doping content. It has been calculated that the total magnetic moment decreases from 4.26 μ_B/f.u. to 4.22 μ_B/f.u. upon 8 at.% Co doping. However, for 2 at.% Co, we observe a significant difference in the local magnetic moment of Fe, in comparison to the corresponding Ni-doped sample. As shown in Fig. 9a, upon 2 at.% Co doping we observe a local moment enhancement on the *3f* site, whereas for 2 at.% Ni doping Fig. 10a indicates a strong weakening of the Fe magnetic moment on the *3f* site, which again is in good agreement with the magnetic measurements discussed in section 3.3.

Table 3
Formation energy calculated per formula unit (eV/f.u.) for Co and Ni substitution.

Site	*Formation energy (Co)*	*Formation energy (Ni)*
3g(Mn)	−4.08490	−4.28724
3g(Fe)	−4.23607	−4.46641
3f(Fe)	−4.38727	−4.51569

The band structure of Co and Ni doped $(Mn,Fe)_2(P,Si)$ for both spin up and spin down channels reveals metallic nature (Fig. S2 and S3 in the Supplementary Material). The observed difference in magnetic behaviour upon Co and Ni doping in $(Mn,Fe)_2(P,Si)$ can be explained by the change in the density of states (DOS) at the Fermi level. The partial DOS for Co and Ni are presented in Fig. 11, whereas the total DOS are shown in Fig. 12. According to ab-initio calculations performed for the doped $(Mn,Fe)_2(P,Si)$ [33], in the Co–doped system, a sharp peak of DOS resides at the Fermi level. This implies that a minor change in the DOS at the Fermi level can result in pronounced changes in magnetic behaviour. The difference between Co and Ni doping is especially highlighted in Fig. 11. Unlike Co-doped $(Mn,Fe)_2(P,Si)$, the DFT calculations did not

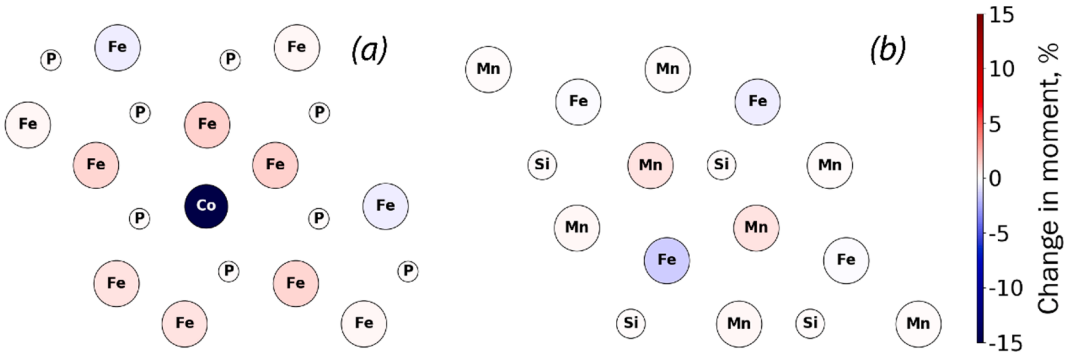

Fig. 9. Change of the local magnetic moment upon 2 at.% Co doping in the (a) *3f* site and (b) *3 g* site. Note that Co prefers the *3f* site.

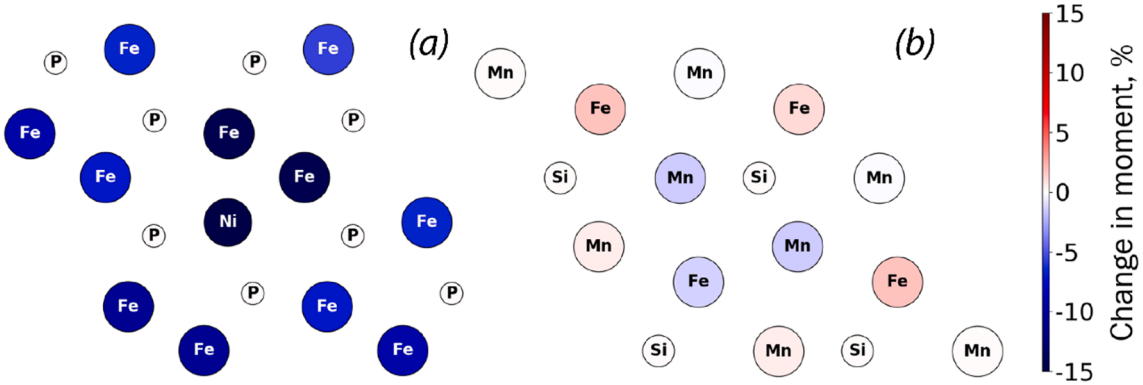

Fig. 10. Change of the local magnetic moment upon 2 at.% Ni doping in the (a) *3f* site and (b) *3 g* site. Note that Ni prefers the *3f* site.

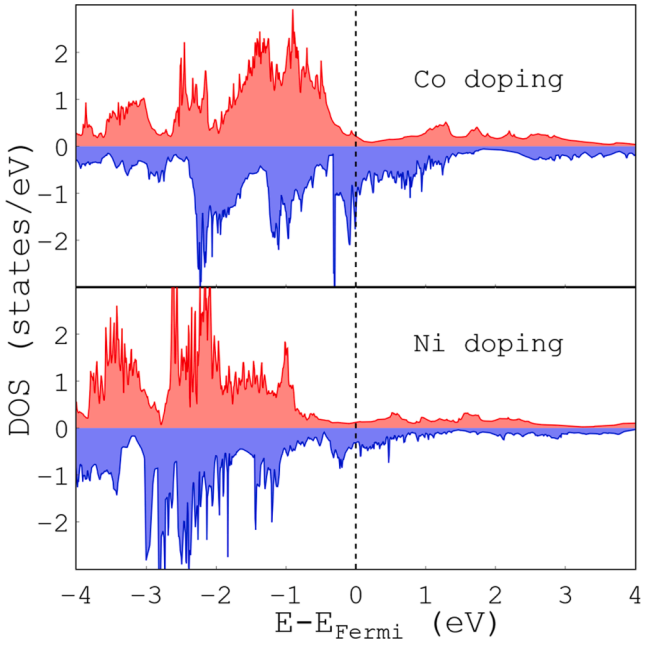

Fig. 11. Partial DOS of $Mn_{0.66}Fe_{1.25}T_{0.08}P_{0.66}Si_{0.33}$ (T = Co, Ni) compounds for Co and Ni in the vicinity of Fermi level. Spin up and spin down states are coloured with red and blue respectively. Zero represents the Fermi energy.

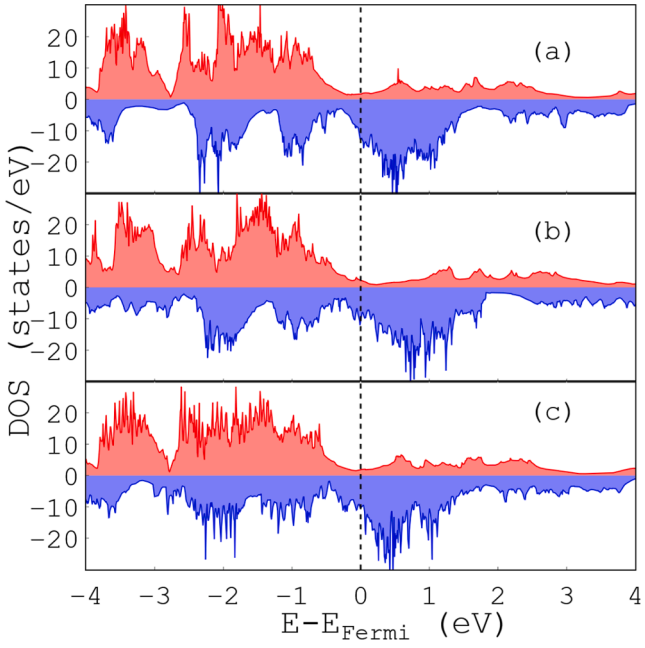

Fig. 12. Total DOS for (a) $Mn_{0.66}Fe_{1.33}P_{0.66}Si_{0.33}$, (b) $Mn_{0.66}Fe_{1.25}Co_{0.08}P_{0.66}Si_{0.33}$ and (c) $Mn_{0.66}Fe_{1.25}Ni_{0.08}P_{0.66}Si_{0.33}$ in the vicinity of Fermi level. Spin up and spin down states are coloured with red and blue respectively. Zero represents the Fermi energy.

predict the presence of a sharp peak at the Fermi level for the Ni-doped system, which indicates that abrupt changes in the magnetic properties are in this case not expected.

4. Conclusions

The $Mn_{0.62-x}Fe_{1.33}Co_xP_{0.66}Si_{0.34}$ and $Mn_{0.62-x}Fe_{1.33}Ni_xP_{0.66}Si_{0.34}$ alloys were prepared by ball-milling and a subsequent solid-state reaction.

The effect of Co and Ni doping on the structure and magnetic properties has been systematically studied using Mössbauer spectroscopy, XRD, EPMA, DSC and magnetization measurements. The obtained results were compared with DFT calculations. All the compounds crystallize in the hexagonal Fe_2P structure with a small amount of the metal-rich $(Mn,Fe)_3Si$ impurity phase for all samples, indicating that further optimization of the $(Mn,Fe)_2(P,Si)$ composition might be important to further optimize the properties. Mössbauer spectroscopy and DFT calculations revealed that the doping atoms substitute Fe at the *3f* site. It is found, that Co and Ni doping both weaken the ferromagnetic ordering and the energy barrier for nucleation, resulting in a decrease in T_c and the thermal hysteresis. On account of the electronic structure of Ni and its preference to the main phase, the decrease in T_c is more pronounced in Ni-doped samples. Although DFT calculations predict a decrease of the total magnetic moment with increasing doping content, an increase in magnetization is observed well above the reference value for 2 at.% of Co. Besides, the DFT calculations show that Co doping, contrary to Ni, enhances the local magnetic moment of Fe atoms at the *3f* site.

CRediT authorship contribution statement

A. Kiecana: Conceptualization, Methodology, Investigation, Writing – original draft. **I. Batashev:** Investigation, Formal analysis, Writing – review & editing. **A.I. Dugulan:** Investigation, Formal analysis. **C. Kwakernaak:** Investigation, Formal analysis. **L. Pieter:** Investigation, Formal analysis. **F. Zhang:** Investigation, Formal analysis. **N.H. Van Dijk:** Conceptualization, Supervision, Writing – review & editing. **E. Brück:** Conceptualization, Supervision, Writing – review & editing.

Declaration of Competing Interest

The authors declare that they have no known competing financial interests or personal relationships that could have appeared to influence the work reported in this paper.

Acknowledgements

The authors would like to acknowledge Anton Lefering, Bert Zwart and Kees Goubitz for their technical assistance. This work was supported by the Dutch Research Council in the framework of Industrial Partnership Programmes IPP 680-91-013, Swiss Blue Energy and RSP Technology.

Appendix A. Supplementary material

Supplementary data to this article can be found online at https://doi.org/10.1016/j.jmmm.2022.169710.

References

[1] E. Brück, Developments in magnetocaloric refrigeration, J. Phys. D: Appl. Phys. 38 (23) (2005) R381–R391.
[2] E. Brück, O. Tegus, D.T.C. Thanh, K.H.J. Buschow, Magnetocaloric refrigeration near room temperature (invited), J. Magn. Magn. Mater. 310 (2) (2007) 2793–2799.
[3] O. Gutfleisch, M.A. Willard, E. Brück, C.H. Chen, S.G. Sankar, J.P. Liu, Magnetic materials and devices for the 21st century: stronger, lighter, and more energy efficient, Adv. Mater. 23 (7) (2011) 821–842, https://doi.org/10.1002/adma.201002180.
[4] A. Gschneidner, V.K. Pecharsky, A.O. Tsokol, Recent developments in magnetocaloric materials, Reports Prog. Phys. 68 (6) (2005) 1479–1539, https://doi.org/10.1088/0034-4885/68/6/R04.
[5] V. Chaudhary, X. Chen, and R. V. Ramanujan, "Iron and manganese based magnetocaloric materials for near room temperature thermal management," *Prog. Mater. Sci.*, vol. 100, no. November 2017, pp. 64–98, 2019, doi: 10.1016/j.pmatsci.2018.09.005.
[6] F. Guillou, G. Porcari, H. Yibole, N. van Dijk, E. Brück, Taming the first-order transition in giant magnetocaloric materials, Adv. Mater. 26 (17) (2014) 2671–2675, https://doi.org/10.1002/adma.201304788.
[7] N.H. Dung, Z.Q. Ou, L. Caron, L. Zhang, D.T.C. Thanh, G.A. de Wijs, R.A. de Groot, K.H.J. Buschow, E. Brück, Mixed magnetism for refrigeration and energy conversion, Adv. Energy Mater. 1 (6) (2011) 1215–1219, https://doi.org/10.1002/aenm.201100252.
[8] N.H. Dung, L. Zhang, Z.Q. Ou, L. Zhao, L. van Eijck, A.M. Mulders, M. Avdeev, E. Suard, N.H. van Dijk, E. Brück, High/low-moment phase transition in hexagonal Mn-Fe-P-Si compounds, Phys. Rev. B 86 (4) (2012), https://doi.org/10.1103/PhysRevB.86.045134.
[9] Z.Q. Ou, L. Zhang, N.H. Dung, L. Caron, E. Brück, Structure, magnetism and magnetocalorics of Fe-rich (Mn, Fe)1.95P1-xSix melt-spun ribbons, J. Alloys Compd. 710 (2017) 446–451, https://doi.org/10.1016/j.jallcom.2017.03.266.
[10] X. F. Miao *et al.*, "Kinetic-arrest-induced phase coexistence and metastability in (Mn,Fe)2(P,Si)," *Phys. Rev. B*, vol. 94, no. 9, 2016, doi: 10.1103/PhysRevB.94.094426.
[11] J. Lai, et al., Combined effect of annealing temperature and vanadium substitution for mangetocaloric Mn1.2-xVxFe0.75P0.5Si0.5 alloys, J. Alloys Compd. 803 (2019) 671–677, https://doi.org/10.1016/j.jallcom.2019.06.239.
[12] J. Lai, X. You, I. Dugulan, B. Huang, J. Liu, M. Maschek, L. van Eijck, N. van Dijk, E. Brück, Tuning the magneto-elastic transition of (Mn, Fe, V)2(P, Si) alloys to low magnetic field applications, J. Alloys Compd. 821 (2020) 153451, https://doi.org/10.1016/j.jallcom.2019.153451.
[13] N.V. Thang, H. Yibole, N.H. van Dijk, E. Brück, Effect of heat treatment conditions on MnFe(P, Si, B) compounds for room-temperature magnetic refrigeration, J. Alloys Compd. 699 (Mar. 2017) 633–637, https://doi.org/10.1016/j.jallcom.2016.12.402.
[14] X.F. Miao, N.V. Thang, L. Caron, H. Yibole, R.I. Smith, N.H. van Dijk, E. Brück, Tuning the magnetoelastic transition in (Mn, Fe)2(P, Si) by B, C, and N doping, Scr. Mater. 124 (2016) 129–132, https://doi.org/10.1016/j.scriptamat.2016.07.015.
[15] N.V. Thang, H. Yibole, X.F. Miao, K. Goubitz, L. van Eijck, N.H. van Dijk, E. Brück, Effect of carbon doping on the structure and magnetic phase transition in (Mn, Fe2(P, Si)), Jom. 69 (8) (2017) 1432–1438, https://doi.org/10.1007/s11837-017-2400-0.
[16] Q. Zhou, Z.G. Zheng, Z.G. Qiu, Y. Hong, Y. Mozharivskyj, D.C. Zeng, Effect of carbon doping on the structure and magnetocaloric properties of Mn1.15Fe0.80P0.50Si0.50 compounds, J. Supercond. Nov. Magn. 32 (12) (2019) 3987–3994, https://doi.org/10.1007/s10948-019-05184-8.
[17] N. van Thang, N. H. van Dijk, and E. Brück, "Tuneable giant magnetocaloric effect in (Mn,Fe)2(P,Si) materials by Co-B and Ni-B co-doping," *Materials (Basel).*, vol. 10, no. 1, 2017, doi: 10.3390/ma10010014.
[18] Z.Q. Ou, N.H. Dung, L. Zhang, L. Caron, E. Torun, N.H. van Dijk, O. Tegus, E. Brück, Transition metal substitution in Fe2P-based MnFe0.95P0.50Si0.50 magnetocaloric compounds, J. Alloys Compd. 730 (2018) 392–398, https://doi.org/10.1016/j.jallcom.2017.09.315.
[19] C. Banza Lubaba Nkulu, L. Casas, V. Haufroid, T. De Putter, N.D. Saenen, T. Kayembe-Kitenge, P. Musa Obadia, D. Kyanika Wa Mukoma, J.-M. Lunda Ilunga, T.S. Nawrot, O. Luboya Numbi, E. Smolders, B. Nemery, Sustainability of artisanal mining of cobalt in DR Congo, Nat. Sustain. 1 (9) (2018) 495–504, https://doi.org/10.1038/s41893-018-0139-4.
[20] H. Wada, T. Takahara, K. Katagiri, T. Ohnishi, K. Soejima, K. Yamashita, Recent progress of magnetocaloric effect and magnetic refrigerant materials of Mn compounds (invited), J. Appl. Phys. 117 (17) (2015) 172606, https://doi.org/10.1063/1.4914120.
[21] M. Fries, L. Pfeuffer, E. Bruder, T. Gottschall, S. Ener, L.V.B. Diop, T. Gröb, K. P. Skokov, O. Gutfleisch, Microstructural and magnetic properties of Mn-Fe-P-Si (Fe2 P-type) magnetocaloric compounds, Acta Mater. 132 (2017) 222–229, https://doi.org/10.1016/j.actamat.2017.04.040.
[22] R.P. Hermann, et al., Mössbauer spectral study of the magnetocaloric FeMnP 1-xAsx compounds, Phys. Rev. B - Condens. Matter Mater. Phys. 70 (21) (2004) 1–9, https://doi.org/10.1103/PhysRevB.70.214425.
[23] J. Rodríguez-Carvajal, Recent advances in magnetic structure determination by neutron powder diffraction, Phys. B Phys. Condens. Matter 192 (1–2) (1993) 55–69, https://doi.org/10.1016/0921-4526(93)90108-I.
[24] J. T. Armstrong, "Quantitative elemental analysis of individual microparticales with electron beam instruments," *Electron Probe Quantization*, pp. 261–285, Jan. 1991.
[25] G. Kresse, J. Hafner, Ab initio molecular dynamics for liquid metals, Phys. Rev. B. Condens. Matter 47 (1) (1993) 558–561, https://doi.org/10.1103/PhysRevB.47.558.
[26] G. Kresse, J. Furthmüller, Efficiency of ab-initio total energy calculations for metals and semiconductors using a plane-wave basis set, Comput. Mater. Sci. 6 (1) (1996) 15–50, https://doi.org/10.1016/0927-0256(96)00008-0.
[27] P.E. Blöchl, Projector augmented-wave method, Phys. Rev. B 50 (24) (Dec. 1994) 17953–17979, https://doi.org/10.1103/PhysRevB.50.17953.
[28] G. Kresse, D. Joubert, From ultrasoft pseudopotentials to the projector augmented-wave method, Phys. Rev. B 59 (3) (Jan. 1999) 1758–1775, https://doi.org/10.1103/PhysRevB.59.1758.
[29] J.P. Perdew, K. Burke, M. Ernzerhof, Generalized gradient approximation made simple, Phys. Rev. Lett. 77 (18) (Oct. 1996) 3865–3868, https://doi.org/10.1103/PhysRevLett.77.3865.
[30] M. Methfessel, A.T. Paxton, High-precision sampling for Brillouin-zone integration in metals, Phys. Rev. B 40 (6) (Aug. 1989) 3616–3621, https://doi.org/10.1103/PhysRevB.40.3616.
[31] M.F.J. Boeije, P. Roy, F. Guillou, H. Yibole, X.F. Miao, L. Caron, D. Banerjee, N. H. van Dijk, R.A. de Groot, E. Brück, Efficient room-temperature cooling with magnets, Chem. Mater. 28 (14) (2016) 4901–4905, https://doi.org/10.1021/acs.chemmater.6b00518.
[32] D. Fruchart, S. Haj-Khlifa, P. de Rango, M. Balli, R. Zach, W. Chajec, P. Fornal, J. Stanek, S. Kaprzyk, J. Tobola, Structure and magnetic properties of bulk

synthesized Mn2−xFexP1−ySiy compounds from magnetization, 57Fe mössbauer spectroscopy, and electronic structure calculations, Crystals 9 (1) (2019) 37, https://doi.org/10.3390/cryst9010037.
[33] P. Roy, E. Torun, and R. A. De Groot, "Effect of doping and elastic properties in (Mn, Fe)2(Si, P)," *Phys. Rev. B*, vol. 93, no. 9, 2016, doi: 10.1103/PhysRevB.93.094110.
[34] N.H. Dung, L. Zhang, Z.Q. Ou, E. Brck, From first-order magneto-elastic to magneto-structural transition in (Mn, Fe)1.95P0.50Si0.50 compounds, Appl. Phys. Lett. 99 (9) (2011), https://doi.org/10.1063/1.3634016.
[35] N.H. Dung, L. Zhang, Z.Q. Ou, E. Brück, Magnetoelastic coupling and magnetocaloric effect in hexagonal Mn-Fe-P-Si compounds, Scr. Mater. 67 (12) (2012) 975–978, https://doi.org/10.1016/j.scriptamat.2012.08.036.
[36] C. Rizal, J. Kolthammer, R.K. Pokharel, B.C. Choi, Magnetic properties of nanostructured Fe-Co alloys, J. Appl. Phys. 113 (11) (2013) 113905, https://doi.org/10.1063/1.4795267.
[37] C. Paduani, J.C. Krause, Electronic structure and magnetization of Fe-Co alloys and multilayers, J. Appl. Phys. 86 (1) (1999) 578–583, https://doi.org/10.1063/1.370769.
[38] V.-T. Tran, C.-C. Fu, K. Li, Predicting magnetization of ferromagnetic binary Fe alloys from chemical short range order, Comput. Mater. Sci. 172 (2020) 109344, https://doi.org/10.1016/j.commatsci.2019.109344.
[39] D. Kim, J. Kim, J. Lee, M.K. Kang, S. Kim, S.H. Park, J. Kim, Y.-H. Choa, J.-H. Lim, Enhanced magnetic properties of FeCo alloys by two-step electroless plating, J. Electrochem. Soc. 166 (4) (2019) D131–D136, https://doi.org/10.1149/2.1251902jes.
[40] E. K. Delczeg-Czirjak *et al.*, "Origin of the magnetostructural coupling in FeMnP0.75 Si0.25," *Phys. Rev. B - Condens. Matter Mater. Phys.*, vol. 90, no. 21, 2014, doi: 10.1103/PhysRevB.90.214436.
[41] H. Yamada, K. Terao, First-order transition of Fe2P and anti-metamagnetic transition, Phase Trans. 75 (1–2) (2002) 231–242, https://doi.org/10.1080/01411590290023120.